

26. Balbus, S. A. & Hawley, J. F. Instability, turbulence, and enhanced transport in accretion discs. *Rev. Mod. Phys.* **70**, 1–53 (1998).
27. Shlosman, I., Begelman, M. C. & Frank, J. The fuelling of active galactic nuclei. *Nature* **345**, 679–686 (1990).
28. Moss, D., Korpi, M., Rautiainen, P. & Salo, H. The evolution of dynamo maintained magnetic fields in a barred spiral galaxy. *Astron. Astrophys.* **329**, 895–905 (1998).
29. Krause, F. & Beck, R. Symmetry and direction of seed magnetic fields in galaxies. *Astron. Astrophys.* **335**, 789–796 (1998).

**Acknowledgements.** This work was supported by DFG, RFBR, PPARC and the University of Newcastle. We thank H. Arp, A. Barth and A. Quillen for providing optical images and for comments, E. M. Berkhuijsen, A. Brandenburg and D. Moss for discussions. We thank the NRAO for observation time and the VLA team for performing absentee observations. The ROSAT project is supported by the German Bundesministerium für Bildung, Wissenschaft und Technologie and the Max-Planck Gesellschaft.

Correspondence and requests for materials should be addressed to R.B. (e-mail: rbeck@mpiffr-bonn.mpg.de).

## Predicted signatures of rotating Bose–Einstein condensates

D. A. Butts & D. S. Rokhsar

Department of Physics, University of California, Berkeley, California 94720-7300, USA and Physical Biosciences Division, Lawrence Berkeley National Laboratory, Berkeley, California 94720, USA

Superfluids are distinguished from normal fluids by their peculiar response<sup>1</sup> to rotation: circulating flow in superfluid helium<sup>2,3</sup>, a strongly coupled Bose liquid, can appear only as quantized vortices<sup>4–6</sup>. The newly created Bose–Einstein condensates<sup>7,9</sup>—clouds of millions of ultracold, weakly interacting alkali-metal atoms that occupy a single quantum state—offer the possibility of investigating superfluidity in the weak-coupling regime. An outstanding question is whether Bose–Einstein condensates exhibit a mesoscopic quantum analogue of the macroscopic vortices in superfluids, and what its experimental signature would be. Here we report calculations of the low-energy states of a rotating, weakly interacting Bose gas. We find a succession of transitions between stable vortex patterns of differing symmetries that are in general qualitative agreement with observations<sup>5</sup> of rotating superfluid helium, a strong-coupling superfluid. Counterintuitively, the angular momentum per particle is not quantized. Some angular momenta are forbidden, corresponding to asymmetrical unstable states that provide a physical mechanism for the entry of vorticity into the condensate.

We can predict the steady states of a confined, rotating dilute Bose gas by calculating the macroscopically occupied condensate wavefunction  $\Psi$  that minimizes the total energy of the gas, either at fixed angular momentum per particle  $l = L_z/N\hbar$  or at fixed angular velocity  $\Omega$ . (Here  $L_z$  is the total angular momentum, and  $N$  is the total number of particles.) We consider axially symmetric harmonic confining traps of the sort typically used in experiments on Bose–Einstein condensates<sup>7–9</sup>, with radial and axial oscillation frequencies  $\omega_r$  and  $\omega_z$ , respectively. The radial frequency sets a maximum angular velocity of rotation, because for  $\Omega > \omega_r$  the trap cannot provide the necessary centripetal force, and the gas flies apart.

Interactions within a dilute Bose gas are dominated by two-particle scattering with a characteristic *s*-wave scattering length, *a*, that can be of either sign. A dimensionless measure of the importance of interatomic collisions relative to the confinement of the trap is the parameter  $\gamma \equiv (2/\pi)^{1/2} aN/\sigma_z$ , where  $\sigma_z$  is the width in the axial direction of the ground state of a single particle in the trap. To find the states of a rotating gas we use a variational approach (see Methods) that is exact in the weakly interacting limit of small  $\gamma$ . We discuss below the relevance of these results for strong coupling. For

current experiments  $\gamma$  is of the order of 10–100, but this ratio can be reduced by decreasing *N*, increasing  $\sigma_z$ , or reducing *a* using the recently discovered Feshbach resonances<sup>10</sup>.

From elementary quantum mechanics, one might expect the stable rotating condensates of a Bose gas confined to an axially symmetric potential to be eigenstates of angular momentum. We find that this is generally not the case. Figure 1 shows rotating zero-temperature condensates for a range of values of angular momentum per particle, *l*. These condensates were determined by numerically minimizing the total energy per particle in the laboratory frame  $E_{\text{lab}}$  (kinetic plus trap plus interaction) for positive  $\gamma$  using a variational condensate, subject to a constraint of fixed angular momentum per particle (see Methods for details).

The rotating condensates exhibit an array of singularities shown as black dots in Fig. 1, which represent vortex lines seen in cross-section. Each zero of  $\Psi$  corresponds to a unit vortex, as all colours are encountered once in rainbow order (that is, phase increases by  $2\pi$ ) as every singularity is encircled. Because the condensate velocity is  $\mathbf{v}_s = (\hbar/M)\nabla\theta$ , where  $\theta$  is the phase of  $\Psi$  (and *M* is the atomic mass), the flow about each singularity is counterclockwise, with quantized circulation  $h/M$ . No doubly charged ( $4\pi$ ) vortices are observed. The patterns shown in Fig. 1 rotate with angular velocity  $\Omega = \partial E_{\text{lab}}/\partial l$ . Only mechanically stable states (with  $\partial^2 E_{\text{lab}}/\partial l^2 > 0$ ) are shown; unstable states are considered below.

A striking feature of the rotating Bose–Einstein condensates (with  $l \neq 1$ ) is their lack of full rotational symmetry. Instead, they have only *p*-fold symmetry, with *p* = 2, 3, 4, 5 and 6, as shown in Fig. 1. The combined PT symmetry of time-reversal (T) followed by parity (P) is retained. The orientation of the vortex array represents a spontaneous breaking of rotational symmetry in response to an

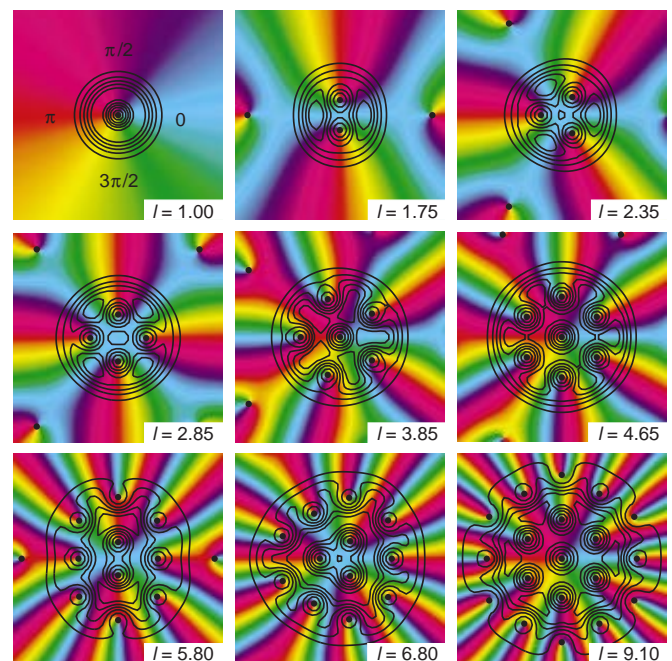


**Figure 1** Rotating condensates. Each panel shows a cross-section perpendicular to the axis of a stably rotating condensate with the indicated angular momentum per particle, *l*. Black lines show density contours. The density of the trapped gas decreases rapidly, and only a radius  $5\sigma_r$  is shown. The phase of the wavefunction is represented by colour, with the colour–phase correspondence shown in the first panel. The characteristic pinwheel patterns that emerge from the zeros of the density (black dots) show that the condensate phase increases by  $2\pi$  as each zero is encircled in an anticlockwise fashion, which implies anticlockwise currents with circulation  $h/M$  about each singularity. In the laboratory frame, these patterns rotate with angular velocity  $\Omega(l)$ .

(arbitrarily weak) asymmetric perturbation of the trap (see below). Because of this symmetry breaking, rotating condensates with  $l \neq 1$  are not eigenstates of angular momentum. The characteristic patterns of these mesoscopic rotating clouds (and the discontinuous transitions between them discussed below) provide a simple yet decisive signature of the quantized vortex network in a mesoscopic superfluid.

To create a vortex from a condensate at rest ( $l = 0$ ), angular momentum must be delivered to the gas. This can be achieved by introducing a weak, steadily rotating asymmetric perturbation of angular frequency  $\Omega$  to exert a torque on the trapped atoms. Such perturbations are now commonly used to excite collective oscillations of the condensate<sup>11,12</sup>. Alternately, specially prepared optical traps<sup>13,14</sup> can be used. The steady states in the presence of a rotating perturbation are those that minimize the energy per particle in the co-rotating frame<sup>15</sup>,  $E_{\text{rot}} \equiv E_{\text{lab}} - \hbar\Omega l$ . Whereas the circulation around any closed path that avoids the singularities is quantized, Fig. 2 shows that the angular momentum per particle is not quantized. For a given symmetry,  $l$  increases smoothly as a function of  $\Omega$ , as the cloud expands to engulf more vortices. The total angular momentum diverges as  $\Omega$  approaches the maximum angular velocity,  $\omega_r$ .

Below a  $\gamma$ -dependent critical angular velocity  $\Omega_{c1}$  the gas does not respond to rotating perturbations, and remains in the non-rotating ground state with  $l = 0$ . At  $\Omega_{c1}$ , the axially symmetric unit vortex ( $l = 1$ ) becomes lower in energy than the  $l = 0$  state in the co-rotating frame, and there is a discontinuous change in the nature of the stable state. For positive  $\gamma$ , we find  $\Omega_{c1} = \omega_r(1 - \gamma/4)$  in the weak coupling limit (see Methods); Baym and Pethick<sup>16</sup> have shown that  $\Omega_{c1}$  varies as  $\omega_r\gamma^{-2/5} \ln \gamma$  for large  $\gamma$ . Stringari and D'Alfovo<sup>17</sup> have demonstrated numerically that  $\Omega_{c1}$  varies smoothly for intermediate  $\gamma$ . For negative  $\gamma$ , however, the results of refs 17 and 18 imply that rotating states are never mechanically stable, as their angular velocities are always greater than, or equal to, the maximum allowable value,  $\omega_r$ . We therefore focus below on positive  $\gamma$ .

A succession of discontinuous, symmetry-changing transitions follows at higher critical velocities  $\Omega_{cn}$ ,  $n = 2, 3, 4, \dots$ , with each

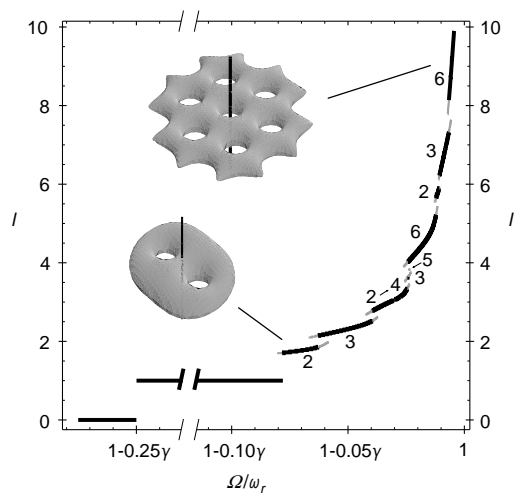


**Figure 2** Angular momentum versus angular velocity. Shown is the angular momentum per particle  $l$  versus the angular velocity  $\Omega/\omega_r$  for stable (black lines) and metastable (thin grey lines) states. There are no stable or metastable states in the forbidden ranges  $l = 0-1$  and  $l = 1-1.70$ . Discontinuities in  $l$  versus  $\Omega$  represent first-order phase transitions between states of different symmetries. The rotational symmetry of each branch is indicated. Three-dimensional plots of surfaces of constant density are shown for states with two-fold and six-fold symmetry in a spherical trap. We note that the clouds become flatter at higher  $\Omega$  due to centrifugal forces.

new stable state corresponding to a different distribution of vortices. The surfaces shown in Fig. 2 (see also Fig. 3 below) make it clear that the discontinuous transitions we observe are topological transformations of the rotating cloud, which develops the appearance of a multi-holed torus. At higher angular velocity, the central arrangement of singularities is well-described as a triangular lattice of vortices whose registry relative to the centre of the trap varies with  $l$  (Fig. 1). Such a vortex lattice is familiar from the well-known behaviour of rotating bulk superfluid helium<sup>19-21</sup>.

We now consider how a trapped Bose–Einstein condensate makes the transition between the stable condensates at  $l = 0$  and  $l = 1$ . Figure 2 shows that there are no mechanically stable states for  $l$  in this interval. Yet the lowest-energy states for these  $l$  are well defined, and can easily be determined by minimizing  $E_{\text{lab}}$ . What are these unstable states of forbidden angular momentum?

States with angular momenta ranging from  $l = 0$  to 1 are shown in Fig. 3. They provide a physical mechanism for the entry of the vortex into the condensate. When the vortex approaches from the periphery of the cloud, the centre of mass of the condensate shifts in the opposite direction, as if repelled by the singularity. This asymmetric distribution of particles orbits the axis with angular velocity  $\Omega_{c1}$  in the laboratory frame, contributing angular momentum from its centre-of-mass motion. Only when the singularity begins to penetrate the cloud does the centre of mass spiral back towards the centre of the trap, eventually returning to the axis.

Transitions between states of differing symmetry are all discontinuous, and generally involve the crossing of an energy barrier. (The  $l = 0 \leftrightarrow l = 1$  transition is an unusual case for which the barrier is zero in the small- $\gamma$  limit, and is more reminiscent of two-phase coexistence.) Barriers imply the existence of mechanically metastable states (that is, local minima of  $E_{\text{rot}}$ ), which are shown as thin grey lines in Fig. 2. As vortices enter the cloud from the low-density periphery, the barrier to incorporating additional vortices is much smaller than in bulk helium, where vortices must be nucleated at the walls of the rotating container, and must overcome the strong image forces exerted by these boundaries. The absence of metastable states at  $\Omega = 0$  implies that the harmonically trapped Bose gas cannot exhibit the phenomenon of persistent currents, because the vortex can slip out of the trap without an energy barrier. (This has also been shown<sup>22</sup> for large  $\gamma$ ). Thus rotating currents are stable only when (1) the gas is driven externally, or (2) in the presence of a pinning potential<sup>23</sup> that stabilizes the  $l \neq 0$  rotating states.

The symmetries of the various rotating states that we have found for a compressible trapped Bose gas, and the sequence in which they appear as a function of  $\Omega$ , agree with the observations<sup>5</sup> of rotating containers of liquid <sup>4</sup>He, which is a strong-coupling superfluid. (The only difference is that in the weak coupling limit studied here, the five-fold symmetric state is metastable.) Thus the phenomena predicted here for trapped dilute gases can be considered as the mesoscopic quantum analogue of the hydrodynamic instabilities

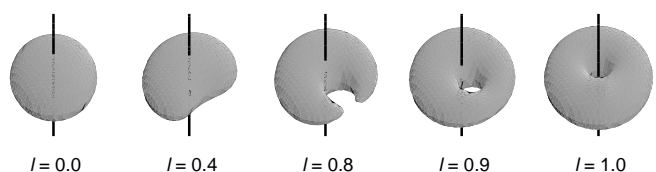


**Figure 3** Mechanism for vortex entry. Panels show surfaces of constant density  $|\Psi(\mathbf{r})|^2$  for a sequence of mechanically unstable states between  $l = 0$  and 1. (The case of a spherically symmetric trap with  $\omega_r = \omega_z$  is shown, but the flattening of the condensate with increasing  $l$  is more general.) The initially spherical cloud is first displaced off-axis as a vortex line approaches. The line is enclosed, and is ultimately drawn back to the centre of the trap. A video of a rotating condensate as it spins up is available at <http://marichal.berkeley.edu/bosemovie>.

found in incompressible inviscid fluids<sup>5,19</sup>. The smooth variation of the properties (such as size and shape<sup>16</sup>, collective mode frequencies<sup>24–26</sup> and thermodynamics<sup>27</sup>) of dilute Bose gases as a function of  $\gamma$ , and the correspondence between our results and the behaviour of rotating liquid <sup>4</sup>He, strongly suggests that the symmetry-breaking phenomena we have described in the weak-coupling limit should occur over the entire range of  $\gamma$  in a qualitatively similar manner.

There are, however, notable quantitative differences. In the small- $\gamma$  limit, we find that the core size and inter-vortex spacing are both comparable to the non-interacting ground-state width  $\sigma_r$ , and that the mean square radial (but not axial) dimension of the cloud grows linearly with  $l$  to accommodate more vortices. In the strong-coupling limit, however, the core size becomes comparable to the healing length  $\xi \approx \sigma_r \gamma^{-1/5}$ , which can be much smaller than the radial extent  $R(0) \approx \sigma_r \gamma^{1/5}$  of the non-rotating cloud<sup>16</sup>. Under these conditions, the spacing between vortices is set by the condition<sup>20</sup> that the mean vorticity (that is, the vortex density) be equal to  $2\Omega$ . An extension of the Thomas–Fermi approach<sup>16</sup> to rapidly rotating gases in the large- $\gamma$  limit then predicts that the radius of the cloud diverges as  $\Omega$  approaches  $\omega_c$ , according to  $R(\Omega) = R(0)\omega_{\text{eff}}^{-3/5}$ , where  $\omega_{\text{eff}} \equiv (\omega_r^2 - \Omega^2)^{1/2}$  is the effective trap frequency, taking centrifugal forces into account. With increasing  $\Omega$  the condensate also flattens, and its axial:radial aspect ratio shrinks as  $Z(\Omega)/R(\Omega) \approx \omega_{\text{eff}}/\omega_r$ , where  $Z(\Omega)$  is the axial extent of the cloud. The angular momentum per particle diverges as  $(\omega_{\text{eff}}/\omega_r)^{-6/5}$ . □

**Methods**

Using the Gross–Pitaevskii approach for trapped Bose gases<sup>16</sup>, we consider variational condensates of the form

$$\Psi(\mathbf{r}) = \sum_{m>0} c_m \chi_m(\mathbf{r}) \tag{1}$$

where the complex coefficients  $c_m$  are the probability amplitudes for finding a condensate atom in the low-energy angular-momentum eigenstates of the harmonic oscillator potential,  $\chi_m(\mathbf{r}) = e^{im\phi} r^m e^{-((r/a)^2 + (z/a_z)^2)/2} / (\pi^{3/2} m! \sigma_r^2 \sigma_z)^{1/2}$ . Here  $\sigma_i \equiv (\hbar/M\omega_i)^{1/2}$  for  $i = r$  or  $z$ ,  $M$  is the atomic mass, and  $\omega_i$  is the oscillation frequency.

The angular momentum per particle in the state (1) is  $lh = \sum |c_m|^2 m \hbar$ , and the kinetic plus trap potential energy per particle is:

$$E_{\text{ideal}}[\Psi] = \sum |c_m|^2 m \hbar \omega_c = lh \omega_c \tag{2}$$

Thus the energy of a rotating non-interacting Bose–Einstein condensate depends only on its angular momentum  $l$ , and not on the detailed form of the superposition (1), indicating a large degeneracy<sup>18</sup>.

In a real gas, interactions between the atoms break this degeneracy and select a particular linear combination to be the lowest energy state for each  $l$ . The Gross–Pitaevskii interaction energy per particle is:

$$E_{\text{int}}[\Psi] \equiv \frac{2\pi \hbar^2 a N}{M} \int |\Psi(\mathbf{r})|^4 d^3\mathbf{r} \tag{3}$$

We have numerically determined the complex amplitudes  $\{c_m\}$  in equation (1) that minimize the total energy in the laboratory frame,  $E_{\text{lab}} = E_{\text{ideal}} + E_{\text{int}}$ , subject to the constraint of fixed angular momentum per particle. Our calculations are exact in the small- $\gamma$  limit, where the use of a single Gross–Pitaevskii condensate is equivalent to degenerate many-body perturbation theory at zero temperature (D.S.R., unpublished results). This result incorporates the effects of small symmetry-breaking perturbations.

The minimum value of  $E_{\text{int}}$  for given  $l$  can be written  $\gamma \hbar \omega_c e_{\text{int}}(l)$ , where  $e_{\text{int}}(l)$  is dimensionless and depends only on the sign of  $\gamma$  for small  $\gamma$ . Then the angular velocity  $\Omega(l) \equiv \partial E_{\text{lab}}/\hbar \partial l = \omega_c (1 + \gamma \partial e_{\text{int}}/\partial l)$ . This function can be inverted to produce  $l(\Omega)$ , which in the weak-coupling limit depends only on  $(\Omega - \omega_c)/\gamma$  (Fig. 2). We note that rotating gases expand (and hence become more dilute) with increasing  $l$ . Thus for positive  $\gamma$  the interaction energy decreases with increasing  $l$ , and we find that  $\Omega(l) < \omega_c$ . For negative  $\gamma$ , however,  $\Omega(l) \geq \omega_c$  for  $l \neq 0$ , and centrifugal forces destabilize all rotating states.

Received 24 July; accepted 5 October 1998.

1. Leggett, A. J. in *Low Temperature Physics* (eds Hoch, M. J. R. & Lemmer, R. H.) 1–92 (Springer, Berlin, 1992).
2. Onsager, L. *Nuovo Cimento* **6**, 249–250 (1949).
3. Feynman, R. F. in *Progress in Low Temperature Physics* Vol. I (ed. Gorter, C. J.) 17–53 (North Holland, Amsterdam, 1955).
4. Vinen, W. F. Single quanta of circulation in helium II. *Proc. R. Soc. Lond. A* **260**, 218–236 (1961).
5. Yarmchuk, E. J., Gordon, M. J. V. & Packard, R. E. Observation of stationary vortex arrays in rotating superfluid helium. *Phys. Rev. Lett.* **43**, 214–217 (1979).
6. Ruutu, V. M. H. *et al.* Vortex formation in neutron-irradiated superfluid <sup>3</sup>He as an analogue for cosmological defect formation. *Nature* **382**, 334–336 (1996).
7. Anderson, M. H., Ensher, J. R., Matthews, M. R., Weiman, C. E. & Cornell, E. A. Observation of Bose-Einstein condensation in a dilute atomic vapor. *Science* **269**, 198–201 (1995).
8. Davis, K. B. *et al.* Bose-Einstein condensation in a gas of sodium atoms. *Phys. Rev. Lett.* **75**, 3969–3973 (1995).
9. Bradley, C. C., Sackett, C. A. & Hulet, R. G. Bose-Einstein condensation of lithium: observation of limited condensate number. *Phys. Rev. Lett.* **78**, 985–989 (1997).
10. Inouye, S. *et al.* Observation of Feshbach resonances in a Bose-Einstein condensate. *Nature* **392**, 151–154 (1998).
11. Jin, D. S., Ensher, J. R., Matthews, M. R., Wieman, C. E. & Cornell, E. A. Collective excitations of a Bose-Einstein condensate in a dilute gas. *Phys. Rev. Lett.* **77**, 420–423 (1996).
12. Mewes, M. O. *et al.* Collective excitations of a Bose-Einstein condensate in a magnetic trap. *Phys. Rev. Lett.* **77**, 988–991 (1996).
13. Marzlin, K., Zhang, W. & Wright, E. M. Vortex coupler for atomic Bose-Einstein condensates. *Phys. Rev. Lett.* **79**, 4728–4731 (1997).
14. Dum, R. & Castin, Y. Creation of dark solitons and vortices in Bose-Einstein condensates. *Phys. Rev. Lett.* **80**, 2972–2975 (1998).
15. Landau, L. D. & Lifshitz, E. M. *Statistical Physics* 3rd edn (Pergamon, Oxford, 1980).
16. Baym, G. & Pethick, C. J. Ground-state properties of magnetically trapped Bose-condensed rubidium gas. *Phys. Rev. Lett.* **76**, 5–8 (1996).
17. Dalfovo, F. & Stringari, S. Bosons in anisotropic traps: ground state and vortices. *Phys. Rev. A* **53**, 2477–2485 (1996).
18. Wilkin, N. K., Gunn, J. M. F. & Smith, R. A. Do attractive bosons condense? *Phys. Rev. Lett.* **80**, 2265–2268 (1998).
19. Hess, G. B. Angular momentum of superfluid helium in a rotating cylinder. *Phys. Rev.* **161**, 189–193 (1967).
20. Hall, H. E. On the rotation of liquid helium II. *Adv. Phys.* **9**, 89–146 (1960).
21. Campbell, L. J. & Ziff, R. M. Vortex patterns and energies in a rotating superfluid. *Phys. Rev. B* **20**, 1886–1902 (1979).
22. Rokhsar, D. S. Vortex stability and persistent currents in trapped Bose gases. *Phys. Rev. Lett.* **79**, 2164–2167 (1997).
23. Rokhsar, D. S. Dilute Bose gas in a torus: vortices and persistent currents. Preprint cond-mat/9709212 at (<http://xxx.lanl.gov>) (1997).
24. Singh, K. G. & Rokhsar, D. S. Collective excitations of a confined Bose condensate. *Phys. Rev. Lett.* **77**, 1667–1670 (1996).
25. Edwards, M. *et al.* Collective excitations of atomic Bose-Einstein condensates. *Phys. Rev. Lett.* **77**, 1671–1674 (1996).
26. Stringari, S. Collective excitations of a trapped Bose-condensed gas. *Phys. Rev. Lett.* **77**, 2360–2363 (1996).
27. Mewes, M. O. *et al.* Bose-Einstein condensation in a tightly confining dc magnetic trap. *Phys. Rev. Lett.* **77**, 416–419 (1996).

**Acknowledgements.** We thank J. C. Davis, A. L. Fetter, R. E. Packard and D. P. Arovos for comments on the manuscript, and the Institute for Theoretical Physics at Santa Barbara for its hospitality while this work was being completed.

Correspondence and requests for materials should be addressed to D.S.R. (e-mail: [rokhsar@physics.berkeley.edu](mailto:rokhsar@physics.berkeley.edu)).

## Cluster-weighted modelling for time-series analysis

N. Gershenfeld\*, B. Schoner\* & E. Metois\*†

\* *Physics and Media Group, MIT Media Laboratory, Cambridge, Massachusetts 02139, USA*

**The need to characterize and forecast time series recurs throughout the sciences, but the complexity of the real world is poorly described by the traditional techniques of linear time-series analysis. Although newer methods can provide remarkable insights into particular domains, they still make restrictive assumptions about the data, the analyst, or the application<sup>1</sup>. Here we show that signals that are nonlinear, non-stationary, non-gaussian, and discontinuous can be described by expanding the probabilistic dependence of the future on the past around local models of their relationship. The predictors derived from**

† Present address: ARIS Technologies, Cambridge, Massachusetts 02140, USA.